EUROPEAN ORGANIZATION FOR NUCLEAR RESEARCH

CERN-PPE/96–24
February 16, 1996

Measurement of Muon-Pair Production at 50 GeV $< \sqrt{s} <$ 86 GeV at LEP

The L3 Collaboration

Abstract

Using the data recorded with the L3 detector at LEP, we study the process $e^+e^- \to \mu^+\mu^-(\gamma)$ for events with hard initial-state photon radiation. The effective centre-of-mass energies of the muons range from 50 GeV to 86 GeV. The data sample corresponds to an integrated luminosity of 103.5 pb^{-1} and yields 293 muon-pair events with a hard photon along the beam direction. The events are used to determine the cross sections and the forward-backward charge asymmetries at centre-of-mass energies below the Z resonance.

Submitted to *Phys. Lett. B*

Introduction

At LEP, the cross sections and forward-backward charge asymmetries for the process $e^+e^- \to \mu^+\mu^-(\gamma)$ are measured at centre-of-mass energies, $\sqrt{s}$, between 88 GeV and 136 GeV [1, 2]. Data from experiments at PEP, PETRA and TRISTAN cover the energy range from 12 GeV to 60 GeV [3]. The energy region between 60 GeV and 88 GeV is not explored by direct measurements, but can be accessed at LEP using events with hard initial-state photon radiation in which the fermion pair is produced at lower centre-of-mass energies [4].

The following analysis uses 93,000 muon-pair events collected with the L3 detector in the years 1991 to 1994. The data correspond to an integrated luminosity of 103.5 pb^{-1}. Events with high missing momentum along the beam direction are interpreted as events with hard initial-state photon radiation. They are used to measure cross sections and forward-backward asymmetries at effective centre-of-mass energies between 50 GeV and 86 GeV.

Photon radiation in fermion-pair production

Radiative corrections to the fermion-pair production process $e^+e^- \to f\bar{f}(\gamma)$ at the Z resonance can be separated into electroweak and QED bremsstrahlung contributions. The electroweak corrections are the sum of propagator, vertex and box corrections, including the effect of the energy dependence of the fine structure constant α. QED bremsstrahlung corrections are present in the initial state (ISR) and final state (FSR). At the Z pole, the interference between initial and final-state radiation is small [5] and allows a separate treatment of both corrections.

In interactions with initial-state bremsstrahlung, a fraction of the beam energy is taken by the photon and the fermion pair is produced at a lower effective centre-of-mass energy, $\sqrt{s'}$. The visible cross section is described by a convolution of the cross section including electroweak corrections, σ_{ew}, with a radiator function, $G(z,s)$,

$$\sigma(s) = \int_{4m_f^2/s}^{1} dz\; G(z,s)\; \sigma_{\mathrm{ew}}(zs)(1+\delta_{\mathrm{FSR}})\;, \tag{1}$$

where $z = s'/s$ [6]. The correction δ_{FSR} is small, *e.g.* 0.17% for $\mu^+\mu^-$ [6], and accounts for the effect of final-state radiation. Measuring the differential cross section of initial-state radiation thus allows to extract the cross section at lower centre-of-mass energies,

$$\frac{d\sigma}{dz} = G(z,s)\;\sigma_{\mathrm{ew}}(zs)\;, \tag{2}$$

since the radiator function $G(z,s)$ is calculable in QED. A first-order calculation [7] for $G(z,s)$ gives

$$G(z,s) = \frac{\alpha}{\pi}\left(\ln\frac{s}{m_e^2} - 1\right)\frac{1+z^2}{1-z}\;. \tag{3}$$

In the analysis presented here the KORALZ Monte Carlo generator [8] is used to take into account higher-order bremsstrahlung corrections. The generator treats the radiation of hard photons in the initial and final state to $\mathcal{O}(\alpha^2)$. The radiation of soft photons is considered in all orders by exponentiation.

Photons are emitted predominantly collinear to the direction of the radiating particles. Initial-state photons go mainly along the direction of the e^+e^- beams, while final-state photons cover the full solid angle. A separation of the different types of radiation is therefore possible.

From the energy, E_γ, of the initial-state photon one finds for the effective centre-of-mass energy squared, s':

$$s' = s\left(1 - 2\frac{E_\gamma}{\sqrt{s}}\right) . \tag{4}$$

For three-particle final states the particle momenta follow from the measured directions using energy and momentum conservation. Assuming that the undetected initial-state photon is radiated in the direction of the beams, its energy is given by the polar angles, θ_1, θ_2, of the outgoing fermions:

$$E_\gamma = \sqrt{s} \cdot \frac{|\sin(\theta_1 + \theta_2)|}{\sin\theta_1 + \sin\theta_2 + |\sin(\theta_1 + \theta_2)|} . \tag{5}$$

Equation (5) cannot be applied to events with more than one hard initial-state photon or in the presence of additional final-state photons which are not collinear with the outgoing fermions. The effect of multiple initial-state photons on the measurement of the cross sections and asymmetries, as well as the final-state photon contamination can be estimated from Monte Carlo simulation.

In this analysis events of the reaction $e^+e^- \to \mu^+\mu^-(\gamma)$ are used. The process allows a clear separation between photons and outgoing leptons and hence gives a good rejection of the final-state bremsstrahlung events. Moreover, the polar angles of the two leptons can be measured with good precision, which is necessary for the determination of s'.

L3 detector

The L3 detector is described in detail in Reference [9]. The components of the detector are the central tracking chamber, the electromagnetic calorimeter composed of bismuth germanium oxide (BGO) crystals with a barrel region ($42^\circ < \theta < 138^\circ$) and two endcaps ($11^\circ < \theta < 37^\circ$ and $143^\circ < \theta < 169^\circ$), a layer of scintillation counters used for time measurements, a fine grained hadron calorimeter with uranium absorbers and proportional wire chamber readout, and a muon spectrometer consisting of three layers of precise drift chambers for the measurement of the transverse muon momentum. The inner and outer muon chamber layers are surrounded with additional layers of drift chambers allowing the measurement of the muon direction in the rz plane and thus a measurement of the polar angle, θ. All sub-detectors are located in a 12 m diameter magnet which provides a uniform field of 0.5 T along the beam direction.

For muons of 45 GeV the three chamber layers allow a momentum measurement with a resolution of 2.5%. The polar angle measurement has a precision of 4.5 mrad which is dominated by multiple scattering of the muon in the calorimeters. Due to the θ resolution the error on $\sqrt{s'}$ according to equations (4) and (5) is smaller than 300 MeV for $\sqrt{s'}$ values between 50 GeV and 86 GeV.

Event selection

The selection of muon-pair events requires two identified muons in the detector. At least one muon must have a reconstructed track in the muon chambers. For the second muon the signature of a minimum ionising particle in the inner detector components [1] is accepted. One muon is restricted to the angular acceptance of the muon chambers $|\cos\theta_\mu| < 0.8$, while for the second a polar angle up to $|\cos\theta_\mu| < 0.9$ is allowed. Background from cosmic rays is removed

by asking a hit in the scintillation counters within a ± 3 ns time window around the beam crossing. In addition, at least one muon must have a track in the inner tracking chamber with a transverse distance of less than 5 mm to the interaction point. To reject hadronic Z decays the calorimetric cluster multiplicity must be less than 15.

For the accepted events we apply equation (5) to calculate the energy, E_γ, of the initial-state photon. Events with a reduced centre-of-mass energy of the muon system, $\sqrt{s'} < 0.95\ \sqrt{s}$, are used for further analysis.

The muon momenta can also be calculated from the polar angles of the muons similarly to the photon energy . A cut on the ratio of the highest measured muon momentum, p_μ, and the momentum, $p_\mu^{\rm exp}$, expected from the polar angles is used to reduce backgrounds from the process $e^+e^- \to \tau^+\tau^-$ and from the two-photon process $e^+e^- \to e^+e^-\mu^+\mu^-$. The distribution of the ratio, $p_\mu/p_\mu^{\rm exp}$ is shown in Figure 1 for data, signal and background Monte Carlo. The cut of $p_\mu/p_\mu^{\rm exp} > 0.8$ removes most of the background.

A Monte Carlo study of the photon reconstruction according Equation (5) is shown in Figure 2. The reconstructed photon energy, E_γ, is compared with the generated photon energy, $E_\gamma^{\rm gen}$. Both energies are normalised to $\sqrt{s}$. Events where a photon is emitted along the beam axis appear in the band A. For these events the photon energy determined from the muon angles reproduces well the generated photon energy, $E_\gamma^{\rm gen}$. For the events of band B a large photon energy is reconstructed, although no photon parallel to the beams is present. A large fraction of these events have a hard photon observed in the detector, mainly originating from final-state radiation. In addition, there are events where a mis-reconstruction of a muon polar-angle leads to a wrong value of E_γ. In the following, the events of region B are considered as background to our signal. They are suppressed by the following cuts:

- The application of Equation (5) is only correct for initial-state photons parallel to the beam axis. Final-state photons can only be accepted if they are collinear with the outgoing muons. Both conditions result a muon pair which is back-to-back in the $r\phi$ plane. The muons are therefore required to have an acoplanarity angle, $\zeta = |\phi_1 - \phi_2 - 180^\circ|$, of less than 2°. The distribution of the muon acoplanarity is shown in Figure 3 for data and Monte Carlo simulation of signal and background.

- Events with a detected photon are only accepted if the transverse energy component of the photon with respect to the direction of the nearest muon is less than 1.5 GeV.

- To ensure the rejection of final-state photons in the acceptance gaps of the electromagnetic calorimeter, events with an energy cluster in the hadron calorimeter of more than 2 GeV and more than 5° away from the nearest muon are rejected.

- The measurement of the muon polar angle using the muon chambers and the polar angle determined from the calorimeters must agree within 2°.

The acceptance, ϵ, for events from the process $e^+e^- \to \mu^+\mu^-\gamma_{\rm ISR}$ is listed in Table 1 for different centre-of-mass energies $\sqrt{s'}$ of the muon system. The quoted values are determined from the Monte Carlo simulation and include the detector efficiency. A large $\sqrt{s'}$ dependence of the acceptance is observed. For lower $\sqrt{s'}$ values the muons are produced at smaller angles to the beam direction and thus fall outside the detector acceptance. The errors on the acceptance reflect the limited Monte Carlo event statistics. Additional systematic errors from the selection cuts and from uncertainties of the detector efficiency are small compared to the statistical error.

The background to the $\mu^+\mu^-\gamma_{\rm ISR}$ signal comes from tau-pair production, $e^+e^- \to \tau^+\tau^-$, from the process, $e^+e^- \to e^+e^-\mu^+\mu^-$, from muon pairs without hard photon radiation, and from events with a final-state photon. The corresponding background fractions $\eta_{\tau\tau}$, $\eta_{ee\mu\mu}$ and $\eta_{\mu\mu}$ respectively are estimated from the Monte Carlo simulation using the KORALZ and DIAG36 [10] generators. To determine the background fraction, $\eta_{\rm FSR}$, of events where the reconstructed photon is radiated from the final state, the four-vector information of a large KORALZ Monte Carlo event sample is used.

Table 2 summarises the four background contributions as fractions of the accepted signal events. The backgrounds from two-photon processes and from events with final-state photons show a significant $\sqrt{s'}$ dependence and are given for the different $\sqrt{s'}$ intervals separately. Within the quoted errors the the values of $\eta_{\tau\tau}$ and $\eta_{\mu\mu}$ are independent of $\sqrt{s'}$.

Cross sections

The data sample used for the cross section measurement was recorded in the years 1991 to 1994 at the three centre-of-mass energies, 89.5 GeV, 91.2 GeV and 93.0 GeV and corresponds to a total integrated luminosity of 103.5 $\rm pb^{-1}$.

The $\sqrt{s'}$ distribution of all selected muon-pair events is shown in Figure 4 in comparison with the Monte Carlo prediction. Good agreement is observed.

Out of this data sample 293 events have a reconstructed $\sqrt{s'}$ value between 50 GeV and 86 GeV and are used to determine the cross section for six energy bins. The number of selected $e^+e^- \to \mu^+\mu^-\gamma_{\rm ISR}$ events, $N_{\mu\mu\gamma}$, are given in Table 3 for the different bins of effective centre-of-mass energy, $\sqrt{s'}$. The observed events are corrected for the expected total background, η ($\eta = \eta_{\tau\tau} + \eta_{ee\mu\mu} + \eta_{\mu\mu} + \eta_{\rm FSR}$), according to Table 2, and the corrected number of events are listed in a second column.

The number of expected initial-state bremsstrahlung events, $N_{\rm ISR}^{\rm MC}$, for the different $\sqrt{s'}$ bins is determined from the Monte Carlo simulation. The luminosity contribution of the three different LEP centre-of-mass energies and the detector efficiency are taken into account. The predictions are given in Table 3.

The cross section, σ, is determined by comparing the background corrected number of $\mu^+\mu^-\gamma_{\rm ISR}$ candidates in the data with the Monte Carlo prediction, $N_{\rm ISR}^{\rm MC}$. The ratio of the two is multiplied by the theoretical cross section, $\sigma_{\rm ew}$, determined from a Standard Model calculation [11]:

$$\sigma(\langle\sqrt{s'}\rangle) = \sigma_{\rm ew}(\langle\sqrt{s'}\rangle) \cdot \frac{N_{\mu\mu\gamma}(1-\eta)}{N_{\rm ISR}^{\rm MC}} \,. \tag{6}$$

The value $\langle\sqrt{s'}\rangle$ is the mean $\sqrt{s'}$ value of the data in the corresponding energy bin. The resulting cross sections for the six different energy points are listed in Table 3. The quoted systematic errors account for the Monte Carlo statistics, uncertainties of the background subtraction and the error on the acceptance determination.

The results are shown in Figure 5 compared with the Standard Model prediction for $\sigma_{\rm ew}$. We also include our results from the cross section measurements around and above the Z-pole energy [1]. They are corrected for the effect of initial-state photon radiation. Our measurement of the cross sections at lower $\sqrt{s'}$ values is in good agreement with the theoretical prediction. For comparison the muon-pair cross sections measured at PEP, PETRA and TRISTAN [3] are also shown. They are corrected to include the effect of the running of the fine structure constant, α.

Forward-backward asymmetries

In the centre-of-mass system of the muons, the angular distribution of the muon-pair production can be parametrised using the forward-backward asymmetry, $A_{\rm fb}$:

$$\frac{d\sigma}{d\cos\theta^*} \propto \left[\tfrac{3}{8}\left(1+\cos^2\theta^*\right) + A_{\rm fb}\cos\theta^*\right] \ . \tag{7}$$

The angle θ^* is the production angle of the μ^- in the centre-of-mass system of the muon pair. In the presence of an initial-state photon, the event is boosted along the beam direction and θ^* can be calculated from the muon polar angles, θ_{μ^-} and θ_{μ^+}, measured in the laboratory:

$$\cos\theta^* = \frac{\sin\frac{1}{2}(\theta_{\mu^+} - \theta_{\mu^-})}{\sin\frac{1}{2}(\theta_{\mu^+} + \theta_{\mu^-})} \ . \tag{8}$$

The forward-backward asymmetry is determined using an unbinned maximum-likelihood fit, where the likelihood, L, is defined as the product of the single-event probabilities:

$$L = \prod_i \left[\tfrac{3}{8}\left(1+\cos^2\theta_i^*\right) + A_{\rm fb}\cos\theta_i^*\right] \ . \tag{9}$$

The result of the fit is shown in Table 4 for the different $\sqrt{s'}$ bins. The asymmetry measurement does not require an accurate knowledge of the luminosity determination or the trigger efficiency. Therefore, the luminosity used for the asymmetry measurement is slightly higher and leads to more events (320 events) than for the cross section measurement. The fitted asymmetry, $A_{\rm fb}^{\rm fit}$, has to be corrected for the background contamination according to Table 2. A correction factor is calculated by assuming a zero asymmetry for the four-fermion production, the Standard Model asymmetry prediction for the tau-pair production, and for the background from muon-pair events without hard photon radiation. The influence of the final-state photon contamination is computed from a high-statistics Monte Carlo event sample by comparing the asymmetry we calculate for the initial-state photon events with the asymmetry value we determine after the full analysis. The correction accounts for the angular distribution of the FSR background, mainly located in the very forward and backward directions, and for the effect of multiple photons. Applying the correction to the fitted asymmetry values we find the forward-backward asymmetry, $A_{\rm fb}$, as given in Table 4. The systematic error reflects the uncertainty of the correction factor.

The results are shown in Figure 6 compared with the Standard Model prediction of the electroweak corrected asymmetry, $A_{\rm fb}^{\rm ew}$. Also shown are our asymmetry measurements around and above the Z-pole energy [1]. They are corrected for the effect of initial-state photon radiation. The measurements of the asymmetry at lower centre-of-mass energies are in good agreement with the theoretical prediction. For comparison, the muon-pair asymmetries measured at PEP, PETRA and TRISTAN [3] are also shown. They are corrected to include the effect of the running of the fine structure constant, α.

Conclusion

The effect of initial-state radiation in the process $e^+e^- \to \mu^+\mu^-(\gamma)$ is studied using 293 events with a hard initial-state photon and an effective centre-of-mass energy between 50 GeV and 86 GeV. The events are used to measure the cross section and the forward-backward asymmetry of the muon-pair production at energies between the TRISTAN and the Z-pole energy. The measurements show good agreement with the Standard Model prediction.

Acknowledgements

We wish to express our gratitude to the CERN accelerator divisions for the excellent performance of the LEP machine. We acknowledge the effort of all engineers and technicians who have participated in the construction and maintenance of this experiment.

References

[1] L3 Collab., M. Acciarri *et al.*, Z. Phys. **C 62** 1994 551;
L3 Collab., M. Acciarri *et al.*, CERN Preprint CERN–PPE/95-191, December 1995.

[2] ALEPH Collab., D. Buskulic *et al.*, Z. Phys. **C 62** (1994) 539;
OPAL Collab., R. Akers *et al.*, Z. Phys. **C 61** (1994) 19;
DELPHI Collab., P. Abreu *et al.*, Nucl. Phys. **B 418** (1994) 403.

[3] HRS Collab., M. Derrick *et al.*, Phys. Rev. **D 31** (1985) 2352;
MAC Collab., W.W. Ash *et al.*, Phys. Rev. Lett. **55** (1985) 1831;
MARK II Collab., M.E. Levi *et al.*, Phys. Rev. Lett. **51** (1983) 1941;
CELLO Collab., H.-J. Behrend *et al.*, Phys. Lett. **B 191** (1987) 209;
JADE Collab., W. Bartel *et al.*, Z. Phys. **C 26** (1985) 507;
MARK J Collab., B. Adeva *et al.*, Phys. Rev. **D 38** (1988) 2665;
PLUTO Collab., Ch. Berger *et al.*, Z. Phys. **C 21** (1983) 53;
TASSO Collab., W. Braunschweig *et al.*, Z. Phys. **C 40** (1988) 163;
AMY Collab., A. Bacala *et al.*, Phys. Lett. **B 331** (1994) 227;
TOPAZ Collab., B. Howell *et al.*, Phys. Lett. **B 291** (1992) 206;
VENUS Colab., K. Abe *et al.*, Z. Phys. **C 48** (1990) 13;
K. Myabayashi,"Recent Electroweak Results from TRISTAN",
Talk presented at the XXXth Rencontre de Moriond, Les Arcs (France) 1995.

[4] OPAL Collab., P. Acton *et al.*, Phys. Lett. **B 273** (1991) 338;
DELPHI Collab., P. Abreu *et al.*, Z. Phys. **C 65** (1995) 603.

[5] S. Jadach and Z. Wąs, Phys. Lett. **B 219** (1989) 103.

[6] F. A. Berends *et al.*, in "Z Physics at LEP 1", Report CERN 89–08 (1989),
eds G. Altarelli, R. Kleiss and C. Verzegnassi, Vol. 1, p. 89.

[7] F.A. Berends, W.L. van Neerven and G.J.H. Burgers, Nucl. Phys. **B 297** (1988) 429.

[8] The KORALZ version 4.01 is used:
S. Jadach, B. F. L. Ward and Z. Wąs, Comp. Phys. Comm. **79** (1994) 503.

[9] L3 Collab., B. Adeva *et al.*, Nucl. Inst. Meth. **A 289** (1990) 35.

[10] F. A. Berends, P. H. Daverfeldt and R. Kleiss, Nucl. Phys. **B 253** (1985) 441.

[11] For the Standard Model calculation the ZFITTER program with $m_{\mathrm{Z}} = 91.195$ GeV, $\alpha_{\mathrm{s}}(m_{\mathrm{Z}}^2) = 0.123$, $m_{\mathrm{t}} = 180$ GeV, $\alpha(m_{\mathrm{Z}}^2) = 1/128.896$ and $m_{\mathrm{H}} = 300$ GeV is used:
D. Bardin *et al.*, FORTRAN package ZFITTER 4.9, and Preprint CERN–TH/6443/92;
D. Bardin *et al.*, Z. Phys. **C 44** (1989) 493;
D. Bardin *et al.*, Nucl. Phys. **B 351** (1991) 1;
D. Bardin *et al.*, Phys. Lett. **B 255** (1991) 290.

The L3 Collaboration:

M.Acciarri,[28] A.Adam,[47] O.Adriani,[17] M.Aguilar-Benitez,[27] S.Ahlen,[11] B.Alpat,[35] J.Alcaraz,[27] G.Alemanni,[23] J.Allaby,[18] A.Aloisio,[30] G.Alverson,[12] M.G.Alviggi,[30] G.Ambrosi,[35] H.Anderhub,[50] V.P.Andreev,[39] T.Angelescu,[13] D.Antreasyan,[9] A.Arefiev,[29] T.Azemoon,[3] T.Aziz,[10] P.Bagnaia,[38] L.Baksay,[45] R.C.Ball,[3] S.Banerjee,[10] K.Banicz,[47] R.Barillère,[18] L.Barone,[38] P.Bartalini,[35] A.Baschirotto,[28] M.Basile,[9] R.Battiston,[35] A.Bay,[23] F.Becattini,[17] U.Becker,[16] F.Behner,[50] J.Berdugo,[27] P.Berges,[16] B.Bertucci,[18] B.L.Betev,[50] M.Biasini,[18] A.Biland,[50] G.M.Bilei[35] J.J.Blaising,[18] S.C.Blyth,[36] G.J.Bobbink,[2] R.Bock,[1] A.Böhm,[1] B.Borgia,[38] A.Boucham,[4] D.Bourilkov,[50] M.Bourquin,[20] D.Boutigny,[4] E.Brambilla,[16] J.G.Branson,[41] V.Brigljevic,[50] I.C.Brock,[36] A.Buijs,[46] A.Bujak,[47] J.D.Burger,[16] W.J.Burger,[20] J.Busenitz,[45] A.Buytenhuijs,[32] X.D.Cai,[19] M.Campanelli,[50] M.Capell,[16] G.Cara Romeo,[9] M.Caria,[35] G.Carlino,[4] A.M.Cartacci,[17] J.Casaus,[27] G.Castellini,[17] R.Castello,[28] F.Cavallari,[38] N.Cavallo,[30] C.Cecchi,[20] M.Cerrada,[27] F.Cesaroni,[24] M.Chamizo,[27] A.Chan,[52] Y.H.Chang,[52] U.K.Chaturvedi,[19] M.Chemarin,[26] A.Chen,[52] C.Chen,[7] G.Chen,[7] G.M.Chen,[7] H.F.Chen,[21] H.S.Chen,[7] M.Chen,[16] G.Chiefari,[30] C.Y.Chien,[5] M.T.Choi,[44] L.Cifarelli,[40] F.Cindolo,[9] C.Civinini,[17] I.Clare,[16] R.Clare,[16] H.O.Cohn,[33] G.Coignet,[4] A.P.Colijn,[2] N.Colino,[27] V.Commichau,[1] S.Costantini,[38] F.Cotorobai,[13] B.de la Cruz,[27] T.S.Dai,[16] R.D'Alessandro,[17] R.de Asmundis,[30] H.De Boeck,[32] A.Degré,[4] K.Deiters,[48] P.Denes,[37] F.DeNotaristefani,[38] D.DiBitonto,[45] M.Diemoz,[38] D.van Dierendonck,[2] F.Di Lodovico,[50] C.Dionisi,[38] M.Dittmar,[50] A.Dominguez,[41] A.Doria,[30] I.Dorne,[4] M.T.Dova,[19,♯] E.Drago,[30] D.Duchesneau,[4] P.Duinker,[2] I.Duran,[42] S.Dutta,[10] S.Easo,[35] Yu.Efremenko,[33] H.El Mamouni,[26] A.Engler,[36] F.J.Eppling,[16] F.C.Erné,[2] J.P.Ernenwein,[26] P.Extermann,[20] M.Fabre,[48] R.Faccini,[38] S.Falciano,[38] A.Favara,[17] J.Fay,[26] M.Felcini,[50] T.Ferguson,[36] D.Fernandez,[27] F.Ferroni,[38] H.Fesefeldt,[1] E.Fiandrini,[35] J.H.Field,[20] F.Filthaut,[36] P.H.Fisher,[16] G.Forconi,[16] L.Fredj,[20] K.Freudenreich,[50] Yu.Galaktionov,[29,16] S.N.Ganguli,[10] S.S.Gau,[12] S.Gentile,[38] J.Gerald,[5] N.Gheordanescu,[13] S.Giagu,[38] S.Goldfarb,[23] J.Goldstein,[11] Z.F.Gong,[21] A.Gougas,[5] G.Gratta,[34] M.W.Gruenewald,[8] V.K.Gupta,[37] A.Gurtu,[10] L.J.Gutay,[47] K.Hangarter,[1] B.Hartmann,[1] A.Hasan,[31] J.T.He,[7] T.Hebbeker,[8] A.Hervé,[18] W.C.van Hoek,[32] H.Hofer,[50] H.Hoorani,[20] S.R.Hou,[52] G.Hu,[19] M.M.Ilyas,[19] V.Innocente,[18] H.Janssen,[4] B.N.Jin,[7] L.W.Jones,[3] P.de Jong,[16] I.Josa-Mutuberria,[27] A.Kasser,[23] R.A.Khan,[19] Yu.Kamyshkov,[33] P.Kapinos,[49] J.S.Kapustinsky,[25] Y.Karyotakis,[4] M.Kaur,[19,◇] M.N.Kienzle-Focacci,[20] D.Kim,[5] J.K.Kim,[44] S.C.Kim,[44] Y.G.Kim,[44] W.W.Kinnison,[25] A.Kirkby,[34] D.Kirkby,[34] J.Kirkby,[18] W.Kittel,[32] A.Klimentov,[16,29] A.C.König,[32] A.Köngeter,[1] I.Korolko,[29] V.Koutsenko,[16,29] A.Koulbardis,[39] R.W.Kraemer,[36] T.Kramer,[16] W.Krenz,[1] H.Kuijten,[32] A.Kunin,[16,29] P.Ladron de Guevara,[27] G.Landi,[17] C.Lapoint,[16] K.Lassila-Perini,[50] M.Lebeau,[18] A.Lebedev,[16] P.Lebrun,[26] P.Lecomte,[50] P.Lecoq,[18] P.Le Coultre,[50] J.S.Lee,[44] K.Y.Lee,[44] C.Leggett,[3] J.M.Le Goff,[18] R.Leiste,[49] M.Lenti,[17] E.Leonardi,[38] P.Levtchenko,[39] C.Li,[21] E.Lieb,[49] W.T.Lin,[52] F.L.Linde,[2,18] B.Lindemann,[1] L.Lista,[30] Z.A.Liu,[7] W.Lohmann,[49] E.Longo,[38] W.Lu,[34] Y.S.Lu,[7] K.Lübelsmeyer,[1] C.Luci,[38] D.Luckey,[16] L.Ludovici,[38] L.Luminari,[38] W.Lustermann,[48] W.G.Ma,[21] A.Macchiolo,[17] M.Maity,[10] G.Majumder,[10] L.Malgeri,[38] A.Malinin,[29] C.Maña,[27] S.Mangla,[10] P.Marchesini,[50] A.Marin,[11] J.P.Martin,[26] F.Marzano,[38] G.G.G.Massaro,[2] K.Mazumdar,[10] D.McNally,[18] S.Mele,[30] L.Merola,[30] M.Meschini,[17] W.J.Metzger,[32] M.von der Mey,[1] Y.Mi,[23] A.Mihul,[13] A.J.W.van Mil,[32] G.Mirabelli,[38] J.Mnich,[18] M.Möller,[1] B.Monteleoni,[17] R.Moore,[3] S.Morganti,[38] R.Mount,[34] S.Müller,[1] F.Muheim,[20] E.Nagy,[14] S.Nahn,[16] M.Napolitano,[30] F.Nessi-Tedaldi,[50] H.Newman,[34] A.Nippe,[1] H.Nowak,[49] G.Organtini,[38] R.Ostonen,[22] D.Pandoulas,[1] S.Paoletti,[38] P.Paolucci,[30] H.K.Park,[36] G.Pascale,[38] G.Passaleva,[17] S.Patricelli,[30] T.Paul,[35] M.Pauluzzi,[35] C.Paus,[1] F.Pauss,[50] D.Peach,[18] Y.J.Pei,[1] S.Pensotti,[28] D.Perret-Gallix,[4] S.Petrak,[8] A.Pevsner,[5] D.Piccolo,[30] M.Pieri,[17] J.C.Pinto,[36] P.A.Piroué,[37] E.Pistolesi,[17] V.Plyaskin,[29] M.Pohl,[50] V.Pojidaev,[29,17] H.Postema,[16] N.Produit,[20] R.Raghavan,[10] G.Rahal-Callot,[50] P.G.Rancoita,[28] M.Rattaggi,[28] G.Raven,[41] P.Razis,[31] K.Read,[33] M.Redaelli,[28] D.Ren,[50] M.Rescigno,[38] S.Reucroft,[12] A.Ricker,[1] S.Riemann,[49] B.C.Riemers,[47] K.Riles,[3] O.Rind,[3] S.Ro,[44] A.Robohm,[50] J.Rodin,[16] F.J.Rodriguez,[27] B.P.Roe,[3] S.Röhner,[1] L.Romero,[27] S.Rosier-Lees,[4] Ph.Rosselet,[23] W.van Rossum,[46] S.Roth,[1] J.A.Rubio,[18] H.Rykaczewski,[50] J.Salicio,[18] E.Sanchez,[27] A.Santocchia,[35] M.E.Sarakinos,[22] S.Sarkar,[10] M.Sassowsky,[1] G.Sauvage,[4] C.Schäfer,[1] V.Schegelsky,[39] S.Schmidt-Kaerst,[1] D.Schmitz,[1] P.Schmitz,[1] M.Schneegans,[4] B.Schoeneich,[49] N.Scholz,[50] H.Schopper,[51] D.J.Schotanus,[32] R.Schulte,[1] K.Schultze,[1] J.Schwenke,[1] G.Schwering,[1] C.Sciacca,[30] D.Sciarrino,[20] J.C.Sens,[52] L.Servoli,[35] S.Shevchenko,[34] N.Shivarov,[43] V.Shoutko,[29] J.Shukla,[25] E.Shumilov,[29] T.Siedenburg,[1] D.Son,[44] A.Sopczak,[49] V.Soulimov,[30] B.Smith,[16] P.Spillantini,[17] M.Steuer,[16] D.P.Stickland,[37] F.Sticozzi,[16] H.Stone,[37] B.Stoyanov,[43] A.Straessner,[1] K.Strauch,[15] K.Sudhakar,[10] G.Sultanov,[19] L.Z.Sun,[21] G.F.Susinno,[20] H.Suter,[50] J.D.Swain,[19] X.W.Tang,[7] L.Tauscher,[6] L.Taylor,[12] Samuel C.C.Ting,[16] S.M.Ting,[16] O.Toker,[35] F.Tonisch,[49] M.Tonutti,[1] S.C.Tonwar,[10] J.Tóth,[14] A.Tsaregorodtsev,[39] C.Tully,[37] H.Tuchscherer,[45] K.L.Tung,[7] J.Ulbricht,[50] U.Uwer,[18] E.Valente,[38] R.T.Van de Walle,[32] I.Vetlitsky,[29] G.Viertel,[50] M.Vivargent,[4] R.Völkert,[49] H.Vogel,[36] H.Vogt,[49] I.Vorobiev,[29] A.A.Vorobyov,[39] An.A.Vorobyov,[39] A.Vorvolakos,[31] M.Wadhwa,[6] W.Wallraff,[1] J.C.Wang,[16] X.L.Wang,[21] Y.F.Wang,[16] Z.M.Wang,[21] A.Weber,[1] F.Wittgenstein,[18] S.X.Wu,[19] S.Wynhoff,[1] J.Xu,[11] Z.Z.Xu,[21] B.Z.Yang,[21] C.G.Yang,[7] X.Y.Yao,[7] J.B.Ye,[21] S.C.Yeh,[52] J.M.You,[36] C.Zaccardelli,[34] An.Zalite,[39] P.Zemp,[50] J.Y.Zeng,[7] Y.Zeng,[1] Z.Zhang,[7] Z.P.Zhang,[21] B.Zhou,[11] G.J.Zhou,[7] Y.Zhou,[3] G.Y.Zhu,[7] R.Y.Zhu,[34] A.Zichichi.[9,18,19]

1 I. Physikalisches Institut, RWTH, D-52056 Aachen, FRG[§]
III. Physikalisches Institut, RWTH, D-52056 Aachen, FRG[§]
2 National Institute for High Energy Physics, NIKHEF, and University of Amsterdam, NL-1009 DB Amsterdam, The Netherlands
3 University of Michigan, Ann Arbor, MI 48109, USA
4 Laboratoire d'Annecy-le-Vieux de Physique des Particules, LAPP,IN2P3-CNRS, BP 110, F-74941 Annecy-le-Vieux CEDEX, France
5 Johns Hopkins University, Baltimore, MD 21218, USA
6 Institute of Physics, University of Basel, CH-4056 Basel, Switzerland
7 Institute of High Energy Physics, IHEP, 100039 Beijing, China
8 Humboldt University, D-10099 Berlin, FRG[§]
9 INFN-Sezione di Bologna, I-40126 Bologna, Italy
10 Tata Institute of Fundamental Research, Bombay 400 005, India
11 Boston University, Boston, MA 02215, USA
12 Northeastern University, Boston, MA 02115, USA
13 Institute of Atomic Physics and University of Bucharest, R-76900 Bucharest, Romania
14 Central Research Institute for Physics of the Hungarian Academy of Sciences, H-1525 Budapest 114, Hungary[‡]
15 Harvard University, Cambridge, MA 02139, USA
16 Massachusetts Institute of Technology, Cambridge, MA 02139, USA
17 INFN Sezione di Firenze and University of Florence, I-50125 Florence, Italy
18 European Laboratory for Particle Physics, CERN, CH-1211 Geneva 23, Switzerland
19 World Laboratory, FBLJA Project, CH-1211 Geneva 23, Switzerland
20 University of Geneva, CH-1211 Geneva 4, Switzerland
21 Chinese University of Science and Technology, USTC, Hefei, Anhui 230 029, China
22 SEFT, Research Institute for High Energy Physics, P.O. Box 9, SF-00014 Helsinki, Finland
23 University of Lausanne, CH-1015 Lausanne, Switzerland
24 INFN-Sezione di Lecce and Universitá Degli Studi di Lecce, I-73100 Lecce, Italy
25 Los Alamos National Laboratory, Los Alamos, NM 87544, USA
26 Institut de Physique Nucléaire de Lyon, IN2P3-CNRS,Université Claude Bernard, F-69622 Villeurbanne, France
27 Centro de Investigaciones Energeticas, Medioambientales y Tecnologicas, CIEMAT, E-28040 Madrid, Spain[♭]
28 INFN-Sezione di Milano, I-20133 Milan, Italy
29 Institute of Theoretical and Experimental Physics, ITEP, Moscow, Russia
30 INFN-Sezione di Napoli and University of Naples, I-80125 Naples, Italy
31 Department of Natural Sciences, University of Cyprus, Nicosia, Cyprus
32 University of Nymegen and NIKHEF, NL-6525 ED Nymegen, The Netherlands
33 Oak Ridge National Laboratory, Oak Ridge, TN 37831, USA
34 California Institute of Technology, Pasadena, CA 91125, USA
35 INFN-Sezione di Perugia and Universitá Degli Studi di Perugia, I-06100 Perugia, Italy
36 Carnegie Mellon University, Pittsburgh, PA 15213, USA
37 Princeton University, Princeton, NJ 08544, USA
38 INFN-Sezione di Roma and University of Rome, "La Sapienza", I-00185 Rome, Italy
39 Nuclear Physics Institute, St. Petersburg, Russia
40 University and INFN, Salerno, I-84100 Salerno, Italy
41 University of California, San Diego, CA 92093, USA
42 Dept. de Fisica de Particulas Elementales, Univ. de Santiago, E-15706 Santiago de Compostela, Spain
43 Bulgarian Academy of Sciences, Central Laboratory of Mechatronics and Instrumentation, BU-1113 Sofia, Bulgaria
44 Center for High Energy Physics, Korea Advanced Inst. of Sciences and Technology, 305-701 Taejon, Republic of Korea
45 University of Alabama, Tuscaloosa, AL 35486, USA
46 Utrecht University and NIKHEF, NL-3584 CB Utrecht, The Netherlands
47 Purdue University, West Lafayette, IN 47907, USA
48 Paul Scherrer Institut, PSI, CH-5232 Villigen, Switzerland
49 DESY-Institut für Hochenergiephysik, D-15738 Zeuthen, FRG
50 Eidgenössische Technische Hochschule, ETH Zürich, CH-8093 Zürich, Switzerland
51 University of Hamburg, D-22761 Hamburg, FRG
52 High Energy Physics Group, Taiwan, China
§ Supported by the German Bundesministerium für Bildung, Wissenschaft, Forschung und Technologie
‡ Supported by the Hungarian OTKA fund under contract number T14459.
♭ Supported also by the Comisión Interministerial de Ciencia y Tecnología
♯ Also supported by CONICET and Universidad Nacional de La Plata, CC 67, 1900 La Plata, Argentina
◇ Also supported by Panjab University, Chandigarh-160014, India

Tables

$\sqrt{s'}$ [GeV]	ϵ [%]
50 – 60	25.2 ± 1.4
60 – 70	31.5 ± 1.3
70 – 75	38.8 ± 1.4
75 – 80	38.7 ± 1.1
80 – 83	41.7 ± 0.9
83 – 86	41.9 ± 0.5

Table 1: Acceptance, ϵ, for the selection of $\mu^+\mu^-\gamma_{\rm ISR}$ events. The values are determined from the Monte Carlo simulation and include the detector efficiency.

$\sqrt{s'}$ [GeV]	$\eta_{ee\mu\mu}$ [%]	$\eta_{\rm FSR}$ [%]
50 – 60	6.8 ± 0.6	1.7 ± 0.3
60 – 70	2.9 ± 0.3	5.5 ± 0.5
70 – 75	1.5 ± 0.3	6.4 ± 0.6
75 – 80	0.9 ± 0.1	8.6 ± 0.5
80 – 83	0.3 ± 0.1	7.9 ± 0.4
83 – 86	0.2 ± 0.1	5.9 ± 0.2

$\sqrt{s'}$ [GeV]	$\eta_{\tau\tau}$ [%]	$\eta_{\mu\mu}$ [%]
50 – 86	1.6 ± 0.7	0.9 ± 0.2

Table 2: Expected background from tau-pair production ($\eta_{\tau\tau}$), from four-fermion production ($\eta_{ee\mu\mu}$), from muon-pair production without hard photon radiation along the beam direction ($\eta_{\mu\mu}$), and from events with final-state photon radiation ($\eta_{\rm FSR}$) as a fraction of the selected events.

$\sqrt{s'}$ [GeV]	$\langle\sqrt{s'}\rangle$ [GeV]	$N_{\mu\mu\gamma}$	$N_{\mu\mu\gamma}(1-\eta)$	$N_{\mathrm{ISR}}^{\mathrm{MC}}$	$\sigma \pm$(stat.)$\pm$(syst.) [pb]
50 – 60	55.4	10	8.9	11.8	$24.9 \pm 7.9 \pm 1.5$
60 – 70	65.8	17	15.3	19.2	$20.3 \pm 4.8 \pm 0.9$
70 – 75	73.3	30	27.2	18.9	$37.1 \pm 6.8 \pm 1.6$
75 – 80	77.9	37	32.6	32.9	$30.5 \pm 5.0 \pm 1.0$
80 – 83	81.7	56	50.6	47.3	$47.8 \pm 6.3 \pm 1.3$
83 – 86	84.8	143	130.7	121.6	$87.5 \pm 7.3 \pm 1.7$

Table 3: Number of selected $e^+e^- \to \mu^+\mu^-\gamma_{\mathrm{ISR}}$ events, $N_{\mu\mu\gamma}$, and the background corrected number, $N_{\mu\mu\gamma}(1-\eta)$. The correction η is the sum of the backgrounds from tau-pair production, from two-photon processes, from muon pairs without photon radiation and from events with final-state photons. Also given are the expected number of initial-state photon events, $N_{\mathrm{ISR}}^{\mathrm{MC}}$. The cross section, σ, is calculated according Equation (6). The systematic error accounts for the Monte Carlo statistics, the uncertainty on the background subtraction and the uncertainty of the efficiency determination. The energy $\langle\sqrt{s'}\rangle$ is the mean energy of the corresponding energy bin.

$\sqrt{s'}$ [GeV]	$\langle\sqrt{s'}\rangle$ [GeV]	N_{f}	N_{b}	$A_{\mathrm{fb}}^{\mathrm{fit}} \pm$(stat.)	$A_{\mathrm{fb}} \pm$(stat.)$\pm$(syst.)
50 – 60	55.0	5	8	-0.14 ± 0.31	$-0.16 \pm 0.36 \pm 0.01$
60 – 70	66.0	7	12	-0.26 ± 0.21	$-0.30 \pm 0.25 \pm 0.01$
70 – 75	73.3	6	24	-0.75 ± 0.17	$-0.84 \pm 0.19 \pm 0.01$
75 – 80	78.0	10	29	-0.52 ± 0.14	$-0.60 \pm 0.17 \pm 0.01$
80 – 83	81.8	16	46	-0.58 ± 0.10	$-0.65 \pm 0.11 \pm 0.01$
83 – 86	84.8	51	106	-0.41 ± 0.07	$-0.44 \pm 0.08 \pm 0.01$

Table 4: Number of forward (N_{f}) and backward (N_{b}) produced muon pairs, the fitted forward-backward asymmetry, $A_{\mathrm{fb}}^{\mathrm{fit}}$, and the resulting background corrected asymmetry value, A_{fb}. The quoted systematic error accounts for the uncertainty of the background correction. The energy $\langle\sqrt{s'}\rangle$ is the mean energy of the corresponding energy bin.

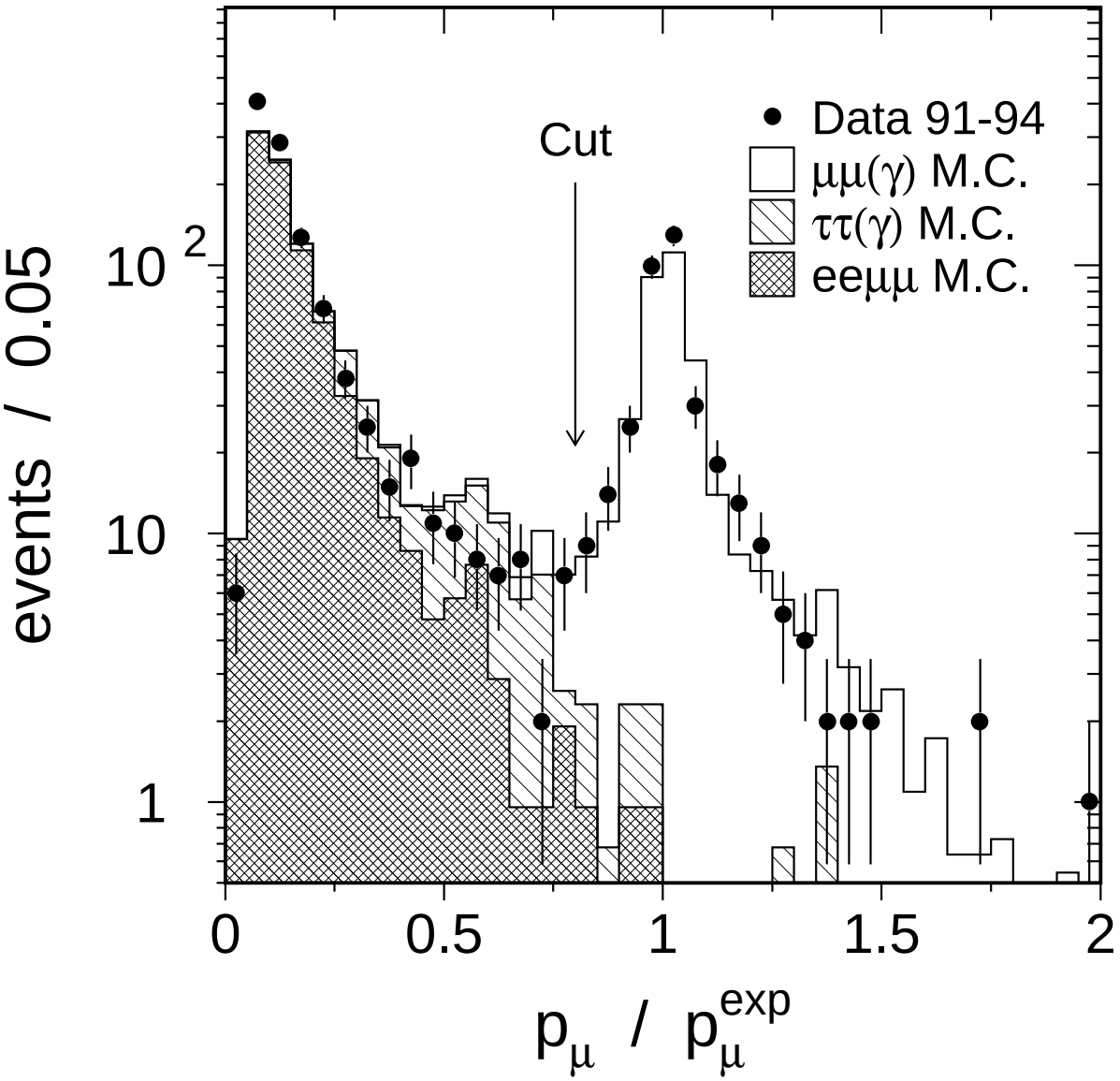

Figure 1: The measured muon momentum, p_μ, normalised to the momentum, $p_\mu^{\rm exp}$, calculated from the polar angles of the muon pair. Data and signal and background Monte Carlo are shown. All other selection cuts are applied.

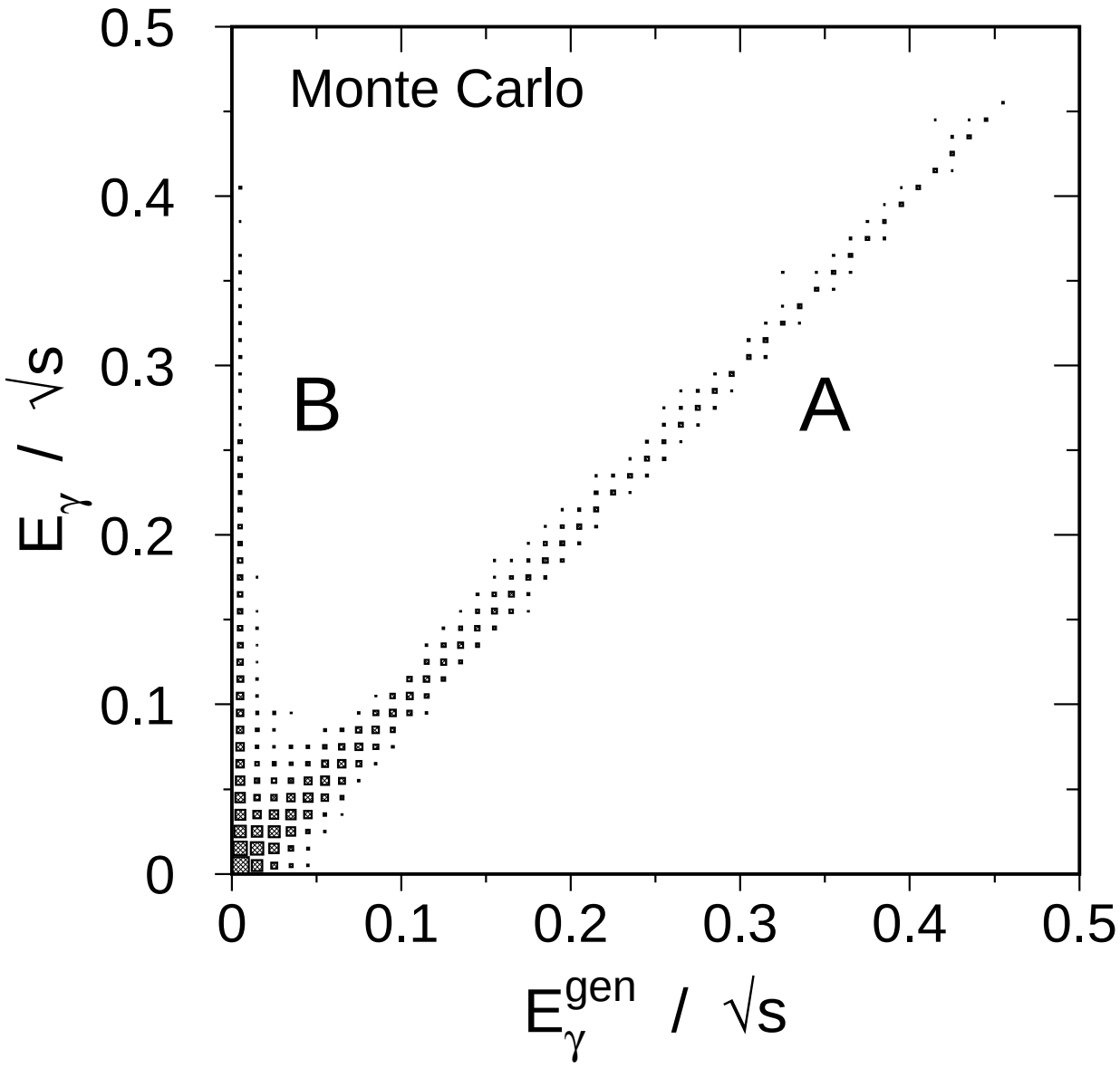

Figure 2: Monte Carlo study of the reconstruction of the photon energy. The reconstructed photon energy, E_γ, using equation (5), is compared with the generated photon energy, $E_\gamma^{\rm gen}$. For the events in the diagonal band A, a photon going along the e^+e^- beams is present. The events of band B, where no hard photon is generated, are regarded as background. The size of the squares is proportional to the logarithm of the number of events.

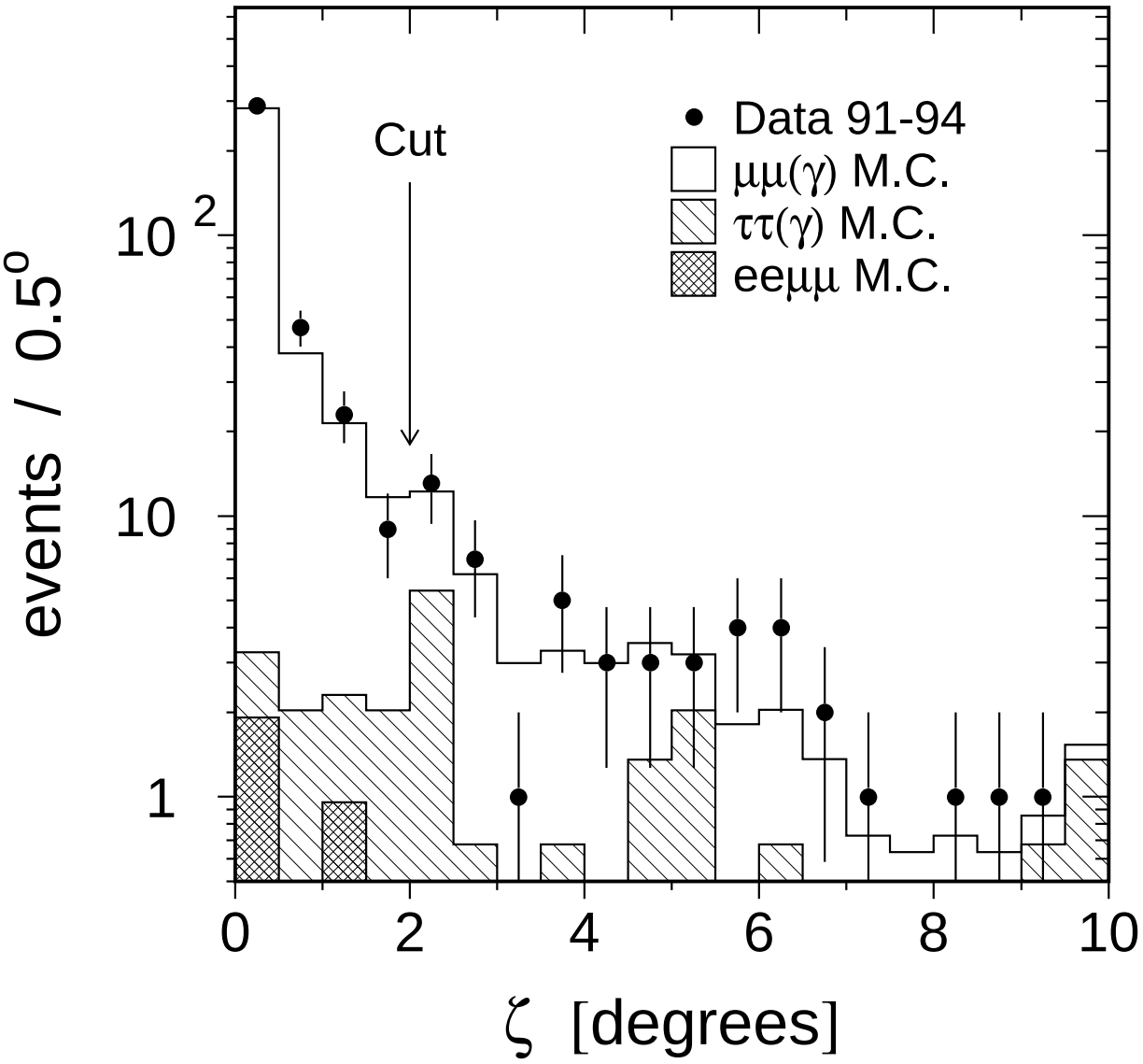

Figure 3: Acoplanarity angle, ζ, of the muon pair for data and signal and background Monte Carlo. All other selection cuts are applied.

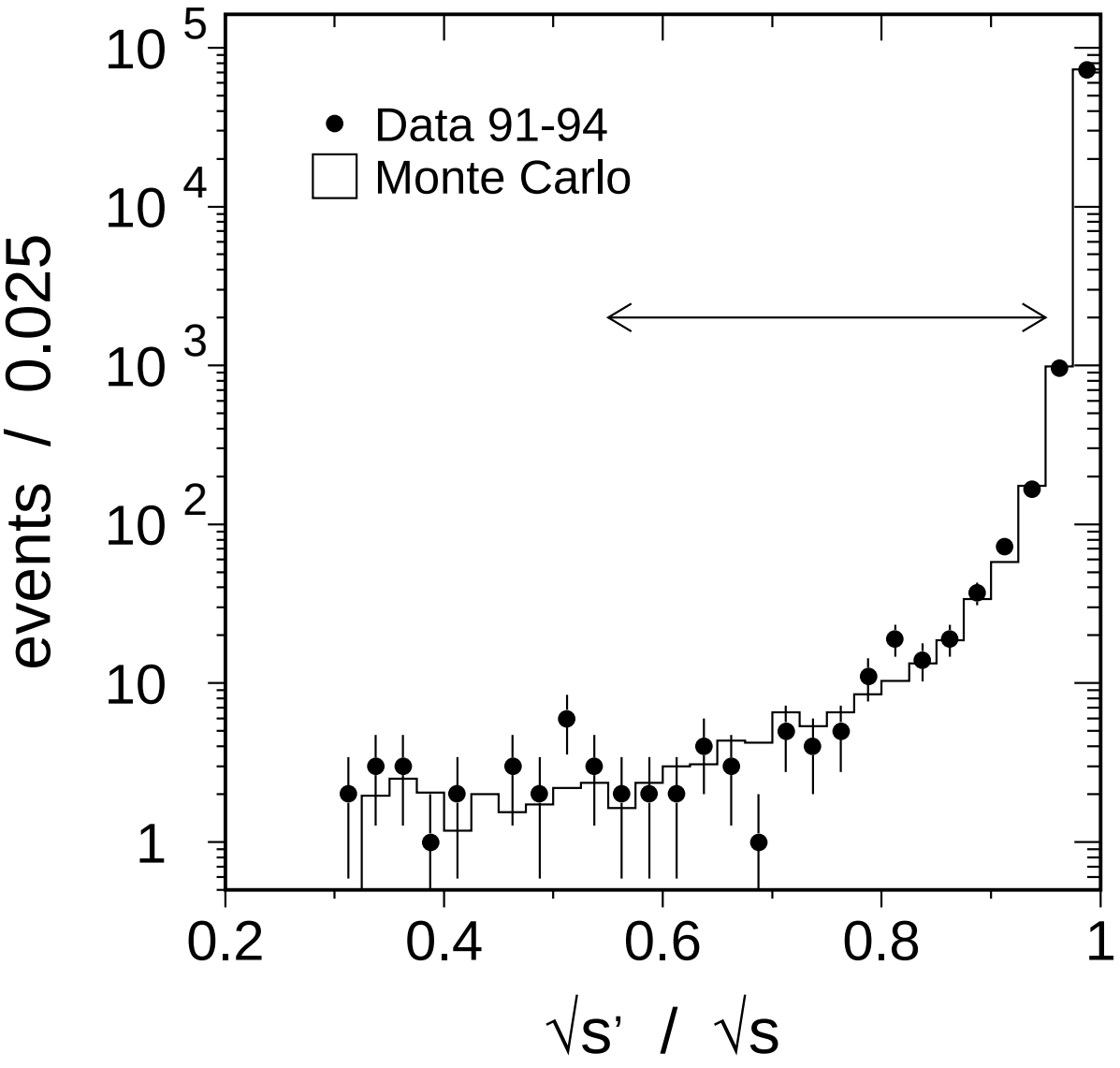

Figure 4: The $\sqrt{s'}$ spectrum of all muon-pair events for data and Monte Carlo simulation. All selection cuts are applied. The double arrow shows the $\sqrt{s'}$ range used for the cross-section and asymmetry measurements (50 GeV $< \sqrt{s'} <$ 86 GeV). In the region $\sqrt{s'}/\sqrt{s} < 0.55$ the background contamination from the two-photon process, $e^+e^- \to e^+e^-\mu^+\mu^-$, becomes large.

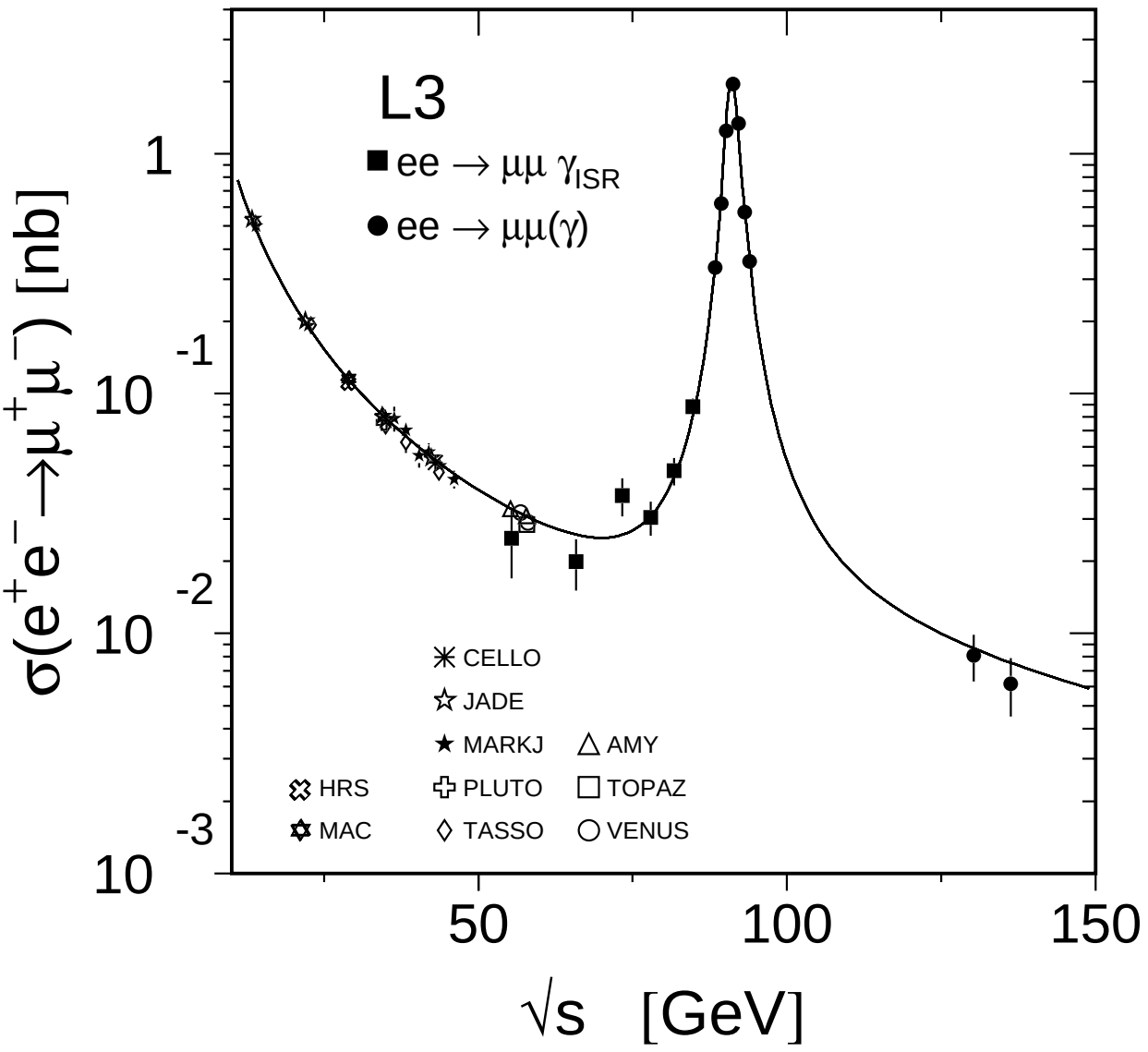

Figure 5: Measured cross sections of muon-pair production compared with the Standard Model prediction. The theory (solid line) does not include the effect of initial-state photon radiation. The results of this analysis, $e^+e^- \to \mu^+\mu^-\gamma_{\rm ISR}$, are shown as solid squares. The L3 results from the measurements at energies around and above the Z pole have been corrected for the effect of initial-state photon radiation and are shown as dots. For comparison the measurements at lower energies from PEP, PETRA and TRISTAN are included.

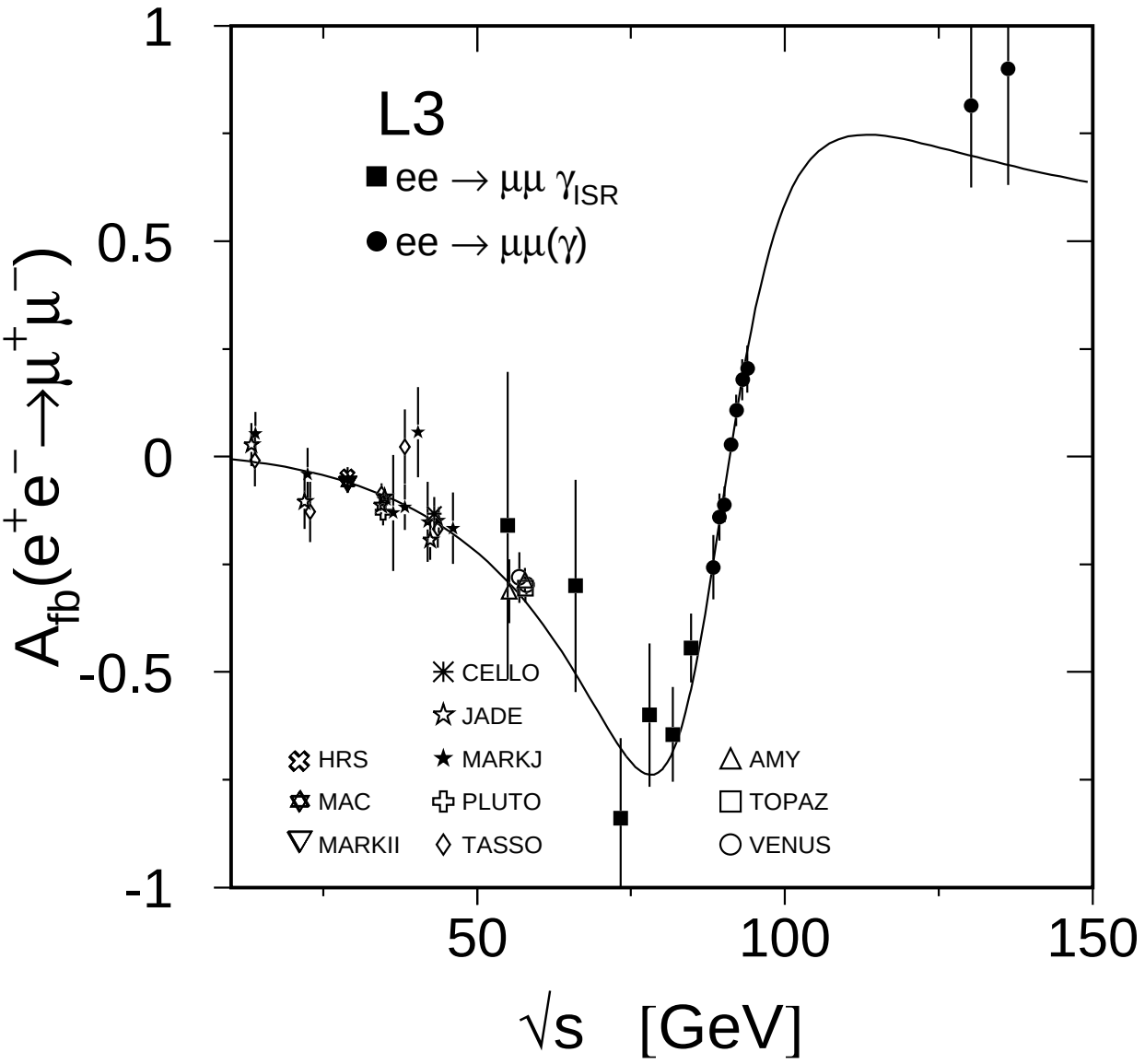

Figure 6: Measured forward-backward asymmetries of muon-pair production compared with Standard Model prediction. The theory (solid line) does not include the effect of initial-state photon radiation. The results of this analysis, $e^+e^- \to \mu^+\mu^-\gamma_{ISR}$, are shown as solid squares. The L3 results from the measurements at energies around and above the Z pole have been corrected for the effect of initial-state photon radiation and are shown as dots. For comparison the measurements at lower energies from PEP, PETRA and TRISTAN are included.